Microglia accelerate the maturation of barrier function of blood brain barrier.	Sato K, Shigemoto-Mogami Y, Hoshikawa K, Sekino Y	SfN2014 (Washington D.C., USA)	2014.11	海外
Search for the human induced pluripotent stem cell-derived neurons capable of detecting the CNS-specific toxicity	Sato K, Takahashi K, Shigemoto-Mogami Y, Ohtsu K, Kanemura Y, Shofuda T, Fukusumi H, Okada Y, Okano H, Shirao T, Sekino Y	SPS 14th annual meeting (Washington D.C., USA)	2014.10	海外
Microglia Enhance Neurogenesis and Oligodendrogenesis in the Early Postnatal Subventricular Zone	Sato K	Dept Cell Biol Anat Seminar, New York medical college (Varhara, USA)	2014.10	海外
Sequential expression of various receptors along with the differentiation of human iPSC-derived neurons	Sato K	ISN satellite symposium (Tokyo, Japan)	2014.9	海外
The Discovery of a Population of Microglia Which Enhance Neurogenesis and Oligodendrogenesis in the Early Postnatal SVZ	Sato K, Shigemoto-Mogami Y, Hoshikawa K, Goldman JE, Sekino Y	9th FENS forum of neuroscicence (Milan, Italy)	2014.7	海外

２．学会誌・雑誌等における論文掲載

掲載した論文（発表題目）	発表者氏名	発表した場所（学会誌・雑誌等名）	発表した時期	国内・外の別
Microglia effects on neuronal development	Sato K (C. A.)	GLIA	in press	海外
Paroxetine prevented the down-regulation of astrocytic L-Glu transporters in neuroinflammation	Fujimori K, Takaki J, Miura M, Shigemoto-Mogami Y, Sekino Y, Suzuki T, Sato K (C. A.)	J Pharamcol Sci	in press	海外
Residual metals in carbon nanotubes suppresses the proliferation of neural stem cells.	Shigemoto-Mogami Y, Fujimori K, Ikarashi Y, Hirose A, Sekino Y, Sato K (C. A.)	Fundam Toxcol Sci, 1(3), 87-94	2014.11	海外
Microglia enhance neurogenesis and oligodendrogenesis in the early postnatal subventricular zone	Shigemoto-Mogami Y, Hoshikawa K, Goldman JE, Sekino Y, Sato K (C. A.)	J Neurosci, 34(5), 2231-2243	2014.1	海外

平成 26 年度厚生労働科学研究委託費

医薬品等規制調和・評価研究事業

IV. 研究成果の刊行物・別刷

Neuroscience Letters 590 (2015) 126–131

Contents lists available at ScienceDirect

Neuroscience Letters

journal homepage: www.elsevier.com/locate/neulet

Research article

An inhibitory pathway controlling the gating mechanism of the mouse lateral amygdala revealed by voltage-sensitive dye imaging

Tomomi Fujieda[a,b], Noriko Koganezawa[b], Yoshinori Ide[a], Tomoaki Shirao[b], Yuko Sekino[a,b,*]

[a] Division of Pharmacology, National Institute of Health Sciences, 1-18-1 Kamiyoga, Setagaya-ku, Tokyo 158-8501, Japan
[b] Department of Neurobiology and Behavior, Gunma University Graduate School of Medicine, 3-39-22 Showa-machi, Maebashi, Gunma 371-8511, Japan

HIGHLIGHTS

- EC stimulation induces large and long-lasting hyperpolarizing signals in the La.
- This hyperpolarization is analyzed by VSD imaging spatially and temporally.
- We identify an inhibitory pathway toward the La via the m-ITC.

ARTICLE INFO

Article history:
Received 14 January 2015
Received in revised form 28 January 2015
Accepted 29 January 2015
Available online 31 January 2015

Keywords:
External capsule
GABAergic neurons
Hyperpolarization
Lateral amygdala
Medial intercalated cluster
Voltage-sensitive dye imaging

ABSTRACT

The lateral amygdala nucleus (La) is known as a gateway for emotional learning that interfaces sensory inputs from the cortex and the thalamus. In the La, inhibitory GABAergic inputs control the strength of sensory inputs and interfere with the initial step of the acquisition of fear memory. In the present study, we investigated the spatial and temporal patterns of the inhibitory responses in mouse La using voltage-sensitive dye imaging. Stimulating the external capsule (EC) induced large and long-lasting hyperpolarizing signals in the La. We focused on these hyperpolarizing signals, revealing the origins of the inhibitory inputs by means of surgical cuts on the possible afferent pathways with four patterns. Isolating the medial branch of EC (ECmed), but not the lateral branch of EC (EClat), from the La strongly suppressed the induction of the hyperpolarization. Interestingly, isolating the ECmed from the caudate putamen did not suppress the hyperpolarization, while the surgical cut of the ECmed fiber tract moderately suppressed it. Glutamatergic antagonists completely suppressed the hyperpolarizing signals induced by the stimulation of EC. When directly stimulating the dorsal, middle or ventral part of the ECmed fiber tract in the presence of glutamatergic antagonists, only the stimulation in the middle part of the ECmed caused hyperpolarization. These data indicate that the GABAergic neurons in the medial intercalated cluster (m-ITC), which receive glutamatergic excitatory input from the ECmed fiber tract, send inhibitory afferents to the La. This pathway might have inhibitory effects on the acquisition of fear memory.

1. Introduction

The amygdala is an important brain structure for emotional behavior and learning [13]. Fear conditioning is a widely-used experimental model to examine emotional and learning processing in animal brains. The lateral amygdala nucleus (La) is known as a gateway for emotional learning that interfaces sensory inputs from the cortex and the thalamus [14]. Inhibitory circuits are known to control the amygdala's functions, such as acquisition, expression, and extinction of conditioned fear [6,21,22]. Inhibitory inputs to the La control the strength of sensory inputs and interfere with the initial step of the acquisition of fear memory. Two groups of GABAergic neurons in the amygdala are known: local interneurons that are scattered within the local neuropil [17], and intercalated cells organized in clusters (intercalated clusters) surrounding the amygdala complex [15,16,18,20,23,24]. Although inhibitory inputs to the individual principal neurons in the amygdala have been analyzed electrophysiologically [4,26,31,37,38], how sensory inputs

* Corresponding author at: Division of Pharmacology, National Institute of Health Sciences, 1-18-1 Kamiyoga, Setagaya-ku, Tokyo 158-8501, Japan.
Tel.: +81 3 3700 9692; fax: +81 3 3700 1452.
E-mail address: yukos@nihs.go.jp (Y. Sekino).

http://dx.doi.org/10.1016/j.neulet.2015.01.079

induce inhibitory responses in the La, and how inhibitory responses propagate in the La, are still unclear because of the technical limitations of patch clamp recording.

Optical imaging techniques overcome these limitations to investigating propagations in a wide range of neuronal interactions, and have been applied in the study of excitatory circuits of several brain regions [7,9,11,12,29,33,34]. In this study, using optical imaging techniques, we investigate neuronal activities in the La, focusing particularly on inhibitory responses. To identify the origins of the inhibitory inputs, we perform various patterns of knife-cut operations of the possible afferent pathways evoking hyperpolarization in the La. In addition, we investigate the effects of glutamatergic antagonists on the inhibitory responses in the La, and show an inhibitory pathway from the medial intercalated cluster (m-lTC) to the La.

2. Materials and methods

2.1. Slice preparation and staining procedure

The experimental protocol was reviewed and approved by the National Institute of Health Sciences (NIHS) in Japan, following the guidelines in the National Research Council's 'Guide for the Care and Use of Laboratory Animals'. All experiments were approved by the NIHS' ethics committee. Male mice (C57BL/6J, 7–22 weeks old, Japan SLC, Inc., Japan) were deeply anesthetized with halothane and quickly decapitated. Coronal slices containing the amygdala complex (400 μm) were prepared using a vibrating microtome (Campden Instruments Ltd., Loughborough, UK) in ice-cold artificial cerebrospinal fluid (ACSF). The ACSF was composed of the following (in mM): 119 NaCl, 2.5 KCl, 1.3 $MgSO_4$, 2.5 $CaCl_2$, 1.0 NaH_2PO_4, 26.2 $NaHCO_3$, and 11.0 glucose; this was oxygenated with a mixture gas of 95% O_2 and 5% CO_2 (pH 7.4). The slices were immediately soaked in the oxygenated ACSF containing a voltage-sensitive dye (VSD), di-4-ANEPPS (50 μM, Invitrogen Molecular Probes Inc., Oregon, USA) for 10 s, and then transferred to a filter that absorbed the staining solution and subsequently to another filter that absorbed the normal ACSF for at least an hour before the experiment.

2.2. Experimental apparatus for VSD imaging

An epi-illumination macro zoom fluorescence microscopy (MVX-10 MacroView, Olympus, Japan), a LED light source with a 530 nm center wavelength (LEX2-Green, Brainvision Inc., Tokyo, Japan), a dichroic mirror (560 nm), an emission filter (BP 575–625 nm), and a CMOS imaging device (MiCAM ULTIMA-L, Brainvision Inc., Tokyo) were used for VSD imaging.

The decrease and increase in the fluorescent intensity from the preparation corresponded to the membrane depolarization and hyperpolarization, respectively. Each data acquisition consisted of 1024 images of consecutive frames (1.0 ms/frame). A coaxial needle electrode (TF203-047, Unique Medical Co. Ltd., Tokyo, Japan) was placed on the external capsule (EC). Electrical stimuli with 200-μs duration at various intensities from 15 to 90 μA were delivered at the 100th frame of each acquisition. To analyze the effects of deafferentation on the induction of the hyperpolarization, the stimulus intensity was adjusted to make the peak value of depolarization equal before and after the surgical cut. Methods to calculate optical signals and present images were described in previous papers [11,29,32].

2.3. Surgical cuts of afferent connections to the La

After recording the optical signals at various stimulation intensities, we performed knife-cut operations on the pathways assumed to be involved in the induction of the hyperpolarization in the La. Four afferent pathways to the La were cut under the macro scope observation, as follows: the La was isolated by the longitudinal cut from: (i) the lateral branch of the EC, (ii) the medial branch of the EC and (iii) the CPu, and by (iv) the transverse cut of ECmed at the dorsal part. For the sham operations, the slices remained intact but the same procedure was carried out. After the surgical cuts, the slices were stored in the recovery chamber at room temperature (at least 1 h).

2.4. Excitation and inhibition values

Images from the 251st–300th frames were stacked and averaged to determine regions of interest (ROIs), which were circles of 8 pixels in diameter. Two ROIs were defined for each experiment. One of the ROIs had the maximal hyperpolarization value in the center spot. The other was adjacent to the first, which had an adequately large hyperpolarization value within the region. For the after-operation analysis, the ROIs were centered on the spots that had the same distances from the position of the stimulating electrode and the EC as the before-operation analysis. The averaged optical signals of the two ROIs were used as representative data.

The excitation (E) value was determined as the largest value among all the values from the first to the 15th frame after electrical stimulation. The inhibition (I) value was determined by averaging 50 frames, from the 251st frame to the 300th frame after the electrical stimulation.

2.5. Statistical analysis

We defined the operation index (OI) as follows: $OI = [I/E]_a/[I/E]_b$, where a: after the operation, b: before the operation. The data were presented as mean ± standard error of the mean (SEM). Normality of the data was tested with the Shapiro–Wilk test, and subsequently one-way ANOVA followed by Dunnett's post-hoc test was carried out. In the pharmacological experiments, inhibition value was statistically analyzed using a paired t-test.

3. Results

3.1. Optical signal propagation after the EC stimulation

The anatomical nomenclatures related to our experiments are shown in Fig. 1A. Each white fiber bundle in the amygdala slice preparation was observed through the macro zoom microscope; thus, the ramifying point of the EC was identified. The La, BLA, and CeA of the amygdala complex were identified in the fluorescent image recorded by the system (Fig. 1B). In Fig. 1C, a typical example of the optical signal propagation is shown in pseudo-color representation. The depolarization started at the stimulation point and spread over the La within 3 ms after the stimulation (0–3 ms). It became stronger in the La and spread over the other regions, the BLA, CPu, and CeA (4–7 ms). Then the depolarization at the dorsal area of the La faded, while growing stronger in the other regions (8–11 ms). Following depolarization, a weak hyperpolarization was first observed in the La; the depolarization remained in the other regions, although it was weakened (12–15 ms). The hyperpolarization grew stronger, and the depolarization in the other regions gradually disappeared (16–19 ms). The hyperpolarization in the La lasted about 600–650 ms (the middle wave in Fig. 1B). The maximal value of the hyperpolarization was observed around 255 ms after the stimulation.

After the hyperpolarization started in the La at the area along the dorsal part of the ECmed (16–19 ms), it spread out in the La during the next 100 ms (20–119 ms), then it spread over the BLA and a narrow part of the CPu along the dorsal part of the ECmed

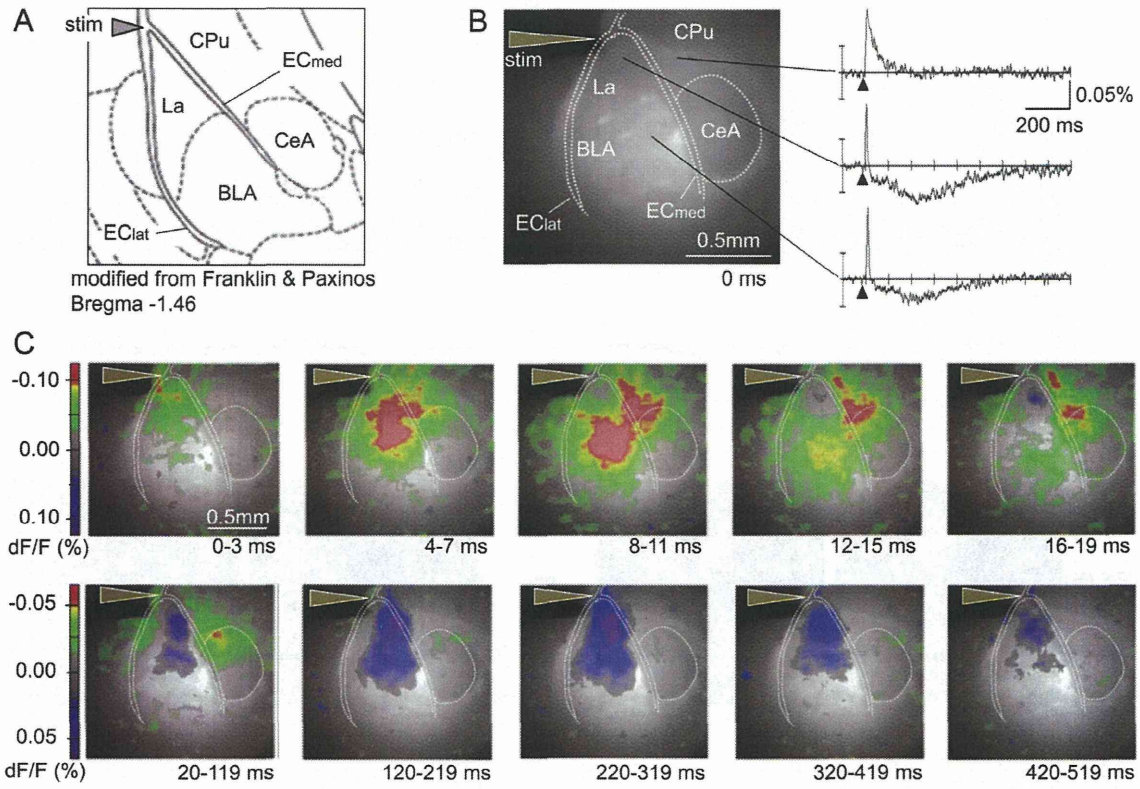

Fig. 1. Optical signal propagation after the EC stimulation.
(A) The modified schematic diagram from the atlas of Franklin and Paxinos (2007) at Bregma −1.46 mm. The arrowhead shows the ramifying point of the external capsule (EC); lateral branch of the external capsule (EClat) and medial branch of the external capsule (ECmed). La – lateral amygdala nucleus; BLA – basolateral amygdala nucleus; CeA – central amygdala nucleus; CPu – caudate putamen. (B) Left, the fluorescence image of VSD-stained coronal slice. Right, a typical example of optical signals in the CPu (in the top wave), La (in the middle wave) and BLA (in the bottom wave). Brown arrowhead, the stimulating site; black arrowhead, the timing of electrical stimulation. (C) Images of optical signal changes produced at the various indicated times after electrical stimulation. In the upper panels, images for 4 frames were stacked to show the spread pattern of depolarization. In the lower panels, images for 100 frames were stacked to show the spread pattern of hyperpolarization.

during the following 100 ms (120–219 ms). The maximal hyperpolarization was observed in the La along the dorsal part of the ECmed from 220 to 319 ms. The strong and long-lasting hyperpolarization was mainly observed in the La (the middle wave in Fig. 1B), while the hyperpolarization in the BLA was weak (the bottom wave). The hyperpolarization was neither observed in the main part of the CPu (the top wave) nor in the CeA, while the depolarization in the CPu lasted longer than in the La and the BLA.

3.2. *Effects of the deafferentation on the optical signals*

To reveal the afferent pathway responsible for evoking the strong and long-lasting hyperpolarization, effects of the various surgical operations were investigated.

Deafferentation from the EClat to the La did not affect the induction of the strong and long-lasting hyperpolarization in the La (Fig 2A), and there was no significant change in the OI value compared with the sham (Fig. 2E), suggesting that the afferent inputs via the EClat are not involved in the hyperpolarization induced in the La. In contrast, deafferentation from the ECmed to the La strongly reduced the hyperpolarization (Fig. 2B). OI values were also significantly reduced (Fig. 2E). These results suggest that the inputs via the ECmed are involved in the hyperpolarization induced in the La.

Next, to investigate the involvement of inputs from the main part of the CPu, we cut off the input from the CPu to the ECmed. In this experiment, the connections between the ECmed and the La remained. The OI values after deafferentation did not significantly change (Fig. 2C and E), suggesting that the inputs from the CPu are not involved in the hyperpolarization induced in the La. For further investigation of the inputs via ECmed, a transverse cut at the dorsal part of the ECmed was carried out. As a result, the hyperpolarization was significantly reduced in the La (Fig. 2D). These data suggest that the fibers running along the ECmed were involved in the induction of hyperpolarization.

3.3. *Effects of glutamatergic antagonists and the source of the inhibition*

Finally, to confirm the details of the inhibitory input source and its properties, the effects of glutamatergic antagonists (6-cyano-7-nitroquinoxaline-2,3-dione (CNQX, 10 μM, TOCRIS), D-(−)-2-amino-5-phosphonopentanoic acid (D-AP5, 50 μM, TOCRIS)) on the inhibitory responses were investigated. The inhibitory responses in the La induced by EC stimulation were statistically significantly reduced after the application of glutamatergic antagonists (Fig. 3A), suggesting that excitatory glutamatergic inputs were involved in the inhibitory response.

We then stimulated several parts along the ECmed in the presence of glutamatergic antagonists (Fig. 3B). Stimulation at the dorsal part of the ECmed did not induce the hyperpolarization (Fig. 3Ba); however, the hyperpolarization could be induced when the middle part of the ECmed was stimulated (Fig. 3Bb). When the electrode moved to the ventral part of the ECmed, weak hyperpolarizing responses were observed (Fig. 3Bc). The magnitude of the hyperpolarization induced by the stimulation at the middle part of the ECmed was statistically significantly larger than that induced by

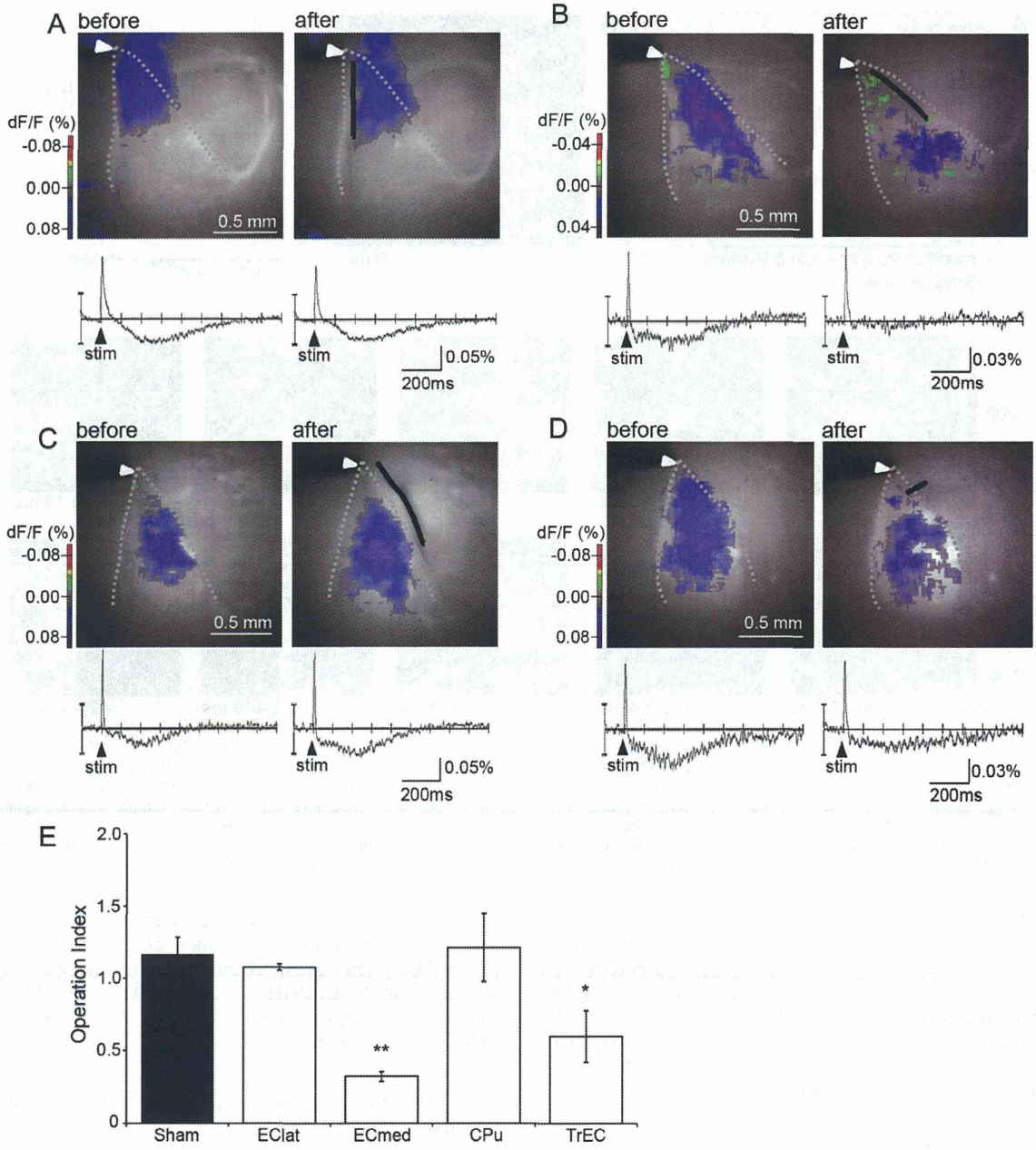

Fig. 2. Effects of deafferentation of the lateral amygdala nucleus on the inhibitory responses.
(A–C) Afferent pathways to the lateral amygdala nucleus were surgically cut from the lateral branch of the external capsule (EClat) in (A), the medial branch (ECmed) in (B), and the caudate putamen (CPu) in (C) to the La was performed, respectively. Black lines, the surgical cut sites; white arrowhead, the stimulating site. The upper images of panels A, B, and C show the spread pattern of hyperpolarization before and after operation. Lower traces, the optical signal traces; black arrowhead, the timing of electrical stimulation. (D) The dorsal part of the ECmed was cut transversely (TrEC). (E) Operation indices (OIs) were quantitatively analyzed among various deafferentations. OIs of ECmed ($n = 6$ slices from 6 mice) and TrEC ($n = 7$ slices from 4 mice) were significantly lower than those of Sham ($n = 5$ slices from 3 mice), EClat ($n = 5$ slices from 4 mice), and CPu ($n = 7$ slices from 4 mice). $^{*}p < 0.05$; $^{**}p < 0.01$.

the stimulation at the other parts (Fig. 3Bd). These results suggest that inhibitory neurons located in the middle part of the ECmed are the main source of the hyperpolarization in the La.

4. Discussion

VSD imaging is a powerful tool to investigate spatial and temporal patterns in the propagation of membrane potential change in the brain tissue. Furthermore, optical signals from the stained slice preparation with VSD are reported to be well-correlated to field EPSPs in vitro [7,8,10,19,25,29,32]. In the amygdala, the signal propagations from the La to the BLA [35,36] and from the La to the CeA have been visualized using VSD imaging [3]. However, these previous studies focused on the propagation of depolarizing signals in the amygdala but not of hyperpolarizing signals.

In the present study, we demonstrated the propagation of the inhibitory responses in the amygdala formation using VSD imaging. The strong and long-lasting hyperpolarization is evoked in the La after the sharp and strong depolarization. In addition, the surgical-cut and the pharmacological experiments indicate that the source of the inhibitory responses is not located in the La or the CPu, but is located in the middle part of the ECmed. According to this

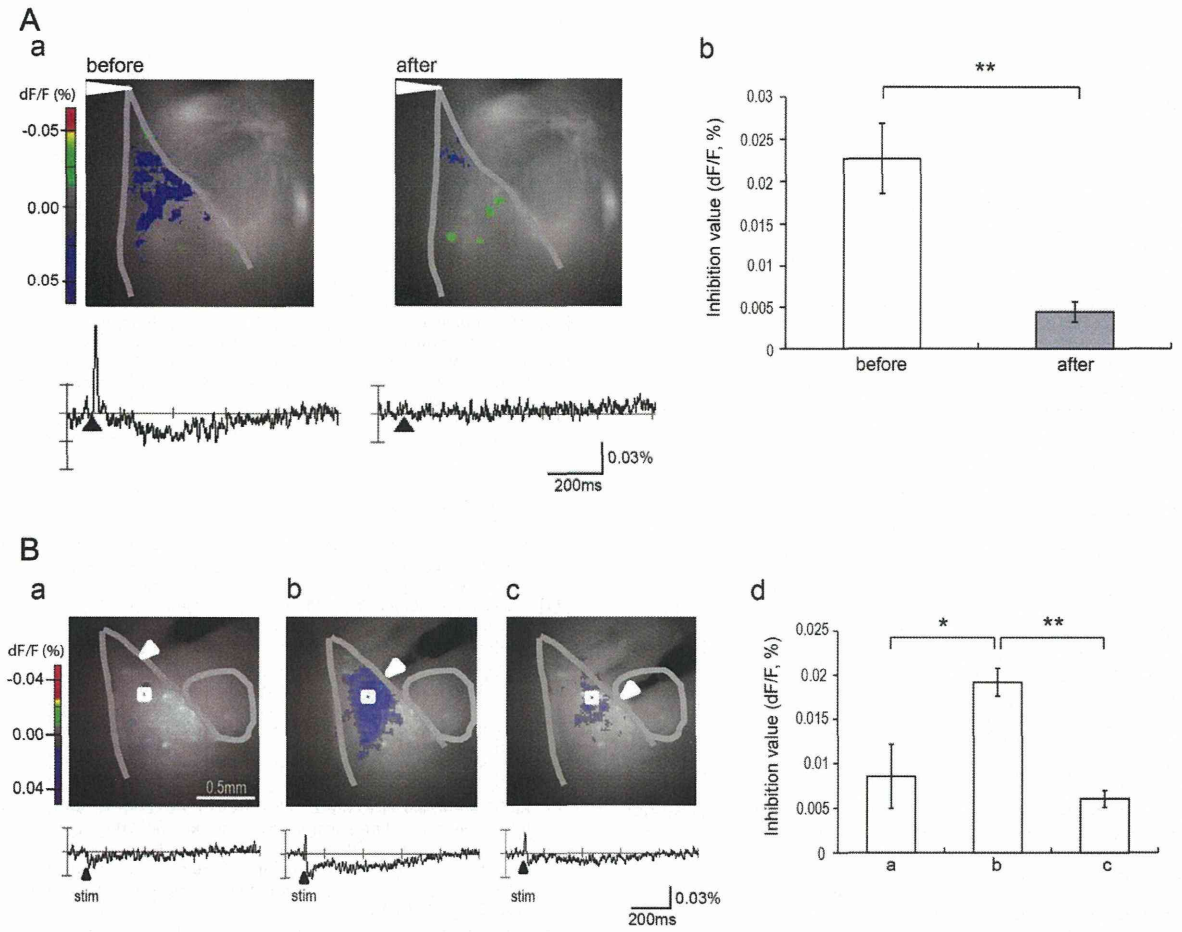

Fig. 3. Effects of glutamatergic antagonists on the inhibitory responses.
(A) The effects of glutamatergic antagonists (CNQX + D-AP5) on the inhibitory response induced by the stimulation of the ramifying point of the external capsule. (Aa) Left and right upper images indicate the spread pattern of hyperpolarization before and after the drug application, respectively. White arrowhead, the stimulating site; lower traces, the optical signal traces; black arrowhead, the timing of electrical stimulation. (Ab) Inhibitory value was statistically compared between before and after CNQX + D-AP5 application ($n = 5$ slices from 5 mice; $^{**}p < 0.01$). (B) The dependence of the stimulus position on inhibitory response of the La in the presence of CNQX + D-AP5. (Ba–c) Upper images indicate the spread pattern of hyperpolarization when the stimulus electrode was at the dorsal, middle, and ventral part of the ECmed, respectively. White arrowhead, the stimulating site; lower traces, the optical signal traces; white squares, the area of which the traces were calculated; black arrowhead, the timing of electrical stimulation. (Bd) Inhibitory value was shown when the stimulus electrode was at the dorsal (a), middle (b), and ventral (c) part of the ECmed ($n = 4$ slices from 4 mice; $^{*}p < 0.05$; $^{**}p < 0.01$).

anatomical location, the source of the inhibitory inputs is likely from the m-ITC in the ECmed [5,18,20,27]. The inhibitory responses were completely eliminated in the presence of the glutamatergic antagonists, indicating that the inhibitory responses are based on the glutamatergic input passing through ECmed. Furthermore, local stimulation of the middle part of the ECmed produces inhibitory responses even in the presence of glutamatergic antagonists, suggesting that GABAergic neurons in the m-ITC are the source of the inhibitory responses of the La. A TrEC cut results in a smaller reduction of the inhibitory responses than an ECmed cut. Because it has been reported that stimulation of the La and the BLA excites the m-ITC neurons [27,28], excitatory glutamatergic inputs to the m-ITC through the La and the BLA might be involved in the inhibitory response in addition to the glutamatergic inputs coming along the ECmed.

In the present study, the contribution of the lateral intercalated clusters located in the EClat was smaller than that of the m-ITC, although the pathway from the lateral intercalated clusters to the BLA has been shown anatomically and electrophysiologically [16,30]. Because the direction of the stimulus electrode used in the present study was from the EClat to the ECmed, resulting in the selective stimulation of the ECmed, the contribution of the lateral intercalated clusters to the inhibitory response in vivo cannot be excluded.

It has been reported that the stimulation of the La and the BLA excites the m-ITC neurons [27,28], resulting in the inhibition of the CeA neurons [2,27]. This pathway is suggested to be involved in the fear extinction mechanism [1], while the inhibitory inputs from m-ITC to La might interfere with the acquisition of fear memory.

In summary, the present study demonstrates the spatial and temporal spread pattern of the inhibitory response in the La after the stimulation of the EC using VSD imaging. Moreover, it is indicated that the inhibitory response is induced via the m-ITC. The pathway from the m-ITC to the La might have inhibitory effects on the acquisition of fear memory.

Acknowledgements

We thank Drs. Miwa and Shimizu for their support. This work was supported by Research Grants from MHLW.

References

[1] T. Amano, C.T. Unal, D. Pare, Synaptic correlates of fear extinction in the amygdala, Nat. Neurosci. 13 (2010) 489–494.
[2] A. Amir, T. Amano, D. Pare, Physiological identification and infralimbic responsiveness of rat intercalated amygdala neurons, J. Neurophysiol. 105 (2011) 3054–3066.
[3] C. Avrabos, S.V. Sotnikov, J. Dine, P.O. Markt, F. Holsboer, R. Landgraf, M. Eder, Real-time imaging of amygdalar network dynamics in vitro reveals a neurophysiological link to behavior in a mouse model of extremes in trait anxiety, J. Neurosci. 33 (2013) 16262–16267.
[4] E.P. Bauer, J.E. LeDoux, Heterosynaptic long-term potentiation of inhibitory interneurons in the lateral amygdala, J. Neurosci. 24 (2004) 9507–9512.
[5] D. Busti, R. Geracitano, N. Whittle, Y. Dalezios, M. Manko, W. Kaufmann, K. Satzler, N. Singewald, M. Capogna, F. Ferraguti, Different fear states engage distinct networks within the intercalated cell clusters of the amygdala, J. Neurosci. 31 (2011) 5131–5144.
[6] I. Ehrlich, Y. Humeau, F. Grenier, S. Ciocchi, C. Herry, A. Luthi, Amygdala inhibitory circuits and the control of fear memory, Neuron 62 (2009) 757–771.
[7] A. Grinvald, L.B. Cohen, S. Lesher, M.B. Boyle, Simultaneous optical monitoring of activity of many neurons in invertebrate ganglia using a 124-element photodiode array, J. Neurophysiol. 45 (1981) 829–840.
[8] A. Grinvald, A. Manker, M. Segal, Visualization of the spread of electrical activity in rat hippocampal slices by voltage-sensitive optical probes, J. Physiol. 333 (1982) 269–291.
[9] T. Iijima, M.P. Witter, M. Ichikawa, T. Tominaga, R. Kajiwara, G. Matsumoto, Entorhinal-hippocampal interactions revealed by real-time imaging, Science 272 (1996) 1176–1179.
[10] W. Jin, R.J. Zhang, J.Y. Wu, Voltage-sensitive dye imaging of population neuronal activity in cortical tissue, J. Neurosci. Methods 115 (2002) 13–27.
[11] M.Z. Kee, J.P. Wuskell, L.M. Loew, G.J. Augustine, Y. Sekino, Imaging activity of neuronal populations with new long-wavelength voltage-sensitive dyes, Brain Cell Biol. 36 (2008) 157–172.
[12] N. Koganezawa, A. Taguchi, T. Tominaga, S. Ohara, K. Tsutsui, M.P. Witter, T. Iijima, Significance of the deep layers of entorhinal cortex for transfer of both perirhinal and amygdala inputs to the hippocampus, Neurosci. Res. 61 (2008) 172–181.
[13] J.E. LeDoux, Emotion circuits in the brain, Annu. Rev. Neurosci. 23 (2000) 155–184.
[14] J.E. LeDoux, P. Cicchetti, A. Xagoraris, L.M. Romanski, The lateral amygdaloid nucleus: sensory interface of the amygdala in fear conditioning, J. Neurosci. 10 (1990) 1062–1069.
[15] D. Marcellino, M. Frankowska, L. Agnati, M. Perez de la Mora, V. Vargas-Barroso, K. Fuxe, J. Larriva-Sahd, Intercalated and paracapsular cell islands of the adult rat amygdala: a combined rapid-Golgi, ultrastructural, and immunohistochemical account, Neuroscience 226 (2012) 324–347.
[16] A. Marowsky, Y. Yanagawa, K. Obata, K.E. Vogt, A specialized subclass of interneurons mediates dopaminergic facilitation of amygdala function, Neuron 48 (2005) 1025–1037.
[17] A.J. McDonald, Neurons of the lateral and basolateral amygdaloid nuclei: a Golgi study in the rat, J. Comp. Neurol. 212 (1982) 293–312.
[18] O.E. Millhouse, The intercalated cells of the amygdala, J. Comp. Neurol. 247 (1986) 246–271.
[19] M. Nakamura, Y. Sekino, T. Manabe, GABAergic interneurons facilitate mossy fiber excitability in the developing hippocampus, J. Neurosci. 27 (2007) 1365–1373.
[20] L. Nitecka, Y. Ben-Ari, Distribution of GABA-like immunoreactivity in the rat amygdaloid complex, J. Comp. Neurol. 266 (1987) 45–55.
[21] H.C. Pape, D. Pare, Plastic synaptic networks of the amygdala for the acquisition, expression, and extinction of conditioned fear, Physiol. Rev. 90 (2010) 419–463.
[22] D. Pare, G.J. Quirk, J.E. Ledoux, New vistas on amygdala networks in conditioned fear, J. Neurophysiol. 92 (2004) 1–9.
[23] D. Pare, Y. Smith, Distribution of GABA immunoreactivity in the amygdaloid complex of the cat, Neuroscience 57 (1993) 1061–1076.
[24] D. Pare, Y. Smith, The intercalated cell masses project to the central and medial nuclei of the amygdala in cats, Neuroscience 57 (1993) 1077–1090.
[25] D. Plenz, A. Aertsen, Current source density profiles of optical recording maps: a new approach to the analysis of spatio-temporal neural activity patterns, Eur. J. Neurosci. 5 (1993) 437–448.
[26] D.G. Rainnie, E.K. Asprodini, P. Shinnick-Gallagher, Inhibitory transmission in the basolateral amygdala, J. Neurophysiol. 66 (1991) 999–1009.
[27] S. Royer, M. Martina, D. Pare, An inhibitory interface gates impulse traffic between the input and output stations of the amygdala, J. Neurosci. 19 (1999) 10575–10583.
[28] S. Royer, M. Martina, D. Pare, Polarized synaptic interactions between intercalated neurons of the amygdala, J. Neurophysiol. 83 (2000) 3509–3518.
[29] Y. Sekino, K. Obata, M. Tanifuji, M. Mizuno, J. Murayama, Delayed signal propagation via CA2 in rat hippocampal slices revealed by optical recording, J. Neurophysiol. 78 (1997) 1662–1668.
[30] Y. Silberman, L. Shi, J.K. Brunso-Bechtold, J.L. Weiner, Distinct mechanisms of ethanol potentiation of local and paracapsular GABAergic synapses in the rat basolateral amygdala, J. Pharmacol. Exp. Ther. 324 (2008) 251–260.
[31] C. Szinyei, T. Heinbockel, J. Montagne, H.C. Pape, Putative cortical and thalamic inputs elicit convergent excitation in a population of GABAergic interneurons of the lateral amygdala, J. Neurosci. 20 (2000) 8909–8915.
[32] T. Tominaga, Y. Tominaga, H. Yamada, G. Matsumoto, M. Ichikawa, Quantification of optical signals with electrophysiological signals in neural activities of Di-4-ANEPPS stained rat hippocampal slices, J. Neurosci. Methods 102 (2000) 11–23.
[33] Y. Tominaga, M. Ichikawa, T. Tominaga, Membrane potential response profiles of CA1 pyramidal cells probed with voltage-sensitive dye optical imaging in rat hippocampal slices reveal the impact of GABA(A)-mediated feed-forward inhibition in signal propagation, Neurosci. Res. 64 (2009) 152–161.
[34] S. Tsuda, M.Z. Kee, C. Cunha, J. Kim, P. Yan, L.M. Loew, G.J. Augustine, Probing the function of neuronal populations: combining micromirror-based optogenetic photostimulation with voltage-sensitive dye imaging, Neurosci. Res. 75 (2013) 76–81.
[35] C. Wang, M.H. Kang-Park, W.A. Wilson, S.D. Moore, Properties of the pathways from the lateral amygdal nucleus to basolateral nucleus and amygdalostriatal transition area, J. Neurophysiol. 87 (2002) 2593–2601.
[36] C. Wang, W.A. Wilson, S.D. Moore, Role of NMDA, non-NMDA, and GABA receptors in signal propagation in the amygdala formation, J. Neurophysiol. 86 (2001) 1422–1429.
[37] A.R. Woodruff, H. Monyer, P. Sah, GABAergic excitation in the basolateral amygdala, J. Neurosci. 26 (2006) 11881–11887.
[38] A.R. Woodruff, P. Sah, Networks of parvalbumin-positive interneurons in the basolateral amygdala, J. Neurosci. 27 (2007) 553–563.

Neurochemistry International 76 (2014) 114–121

Contents lists available at ScienceDirect

Neurochemistry International

journal homepage: www.elsevier.com/locate/nci

Histone deacetylase mediates the decrease in drebrin cluster density induced by amyloid beta oligomers

Yuta Ishizuka [a], Hideo Shimizu [a], Eiko Takagi [a], Mai Kato [a], Hirotaka Yamagata [b], Masahiko Mikuni [c], Tomoaki Shirao [a,*]

[a] Department of Neurobiology and Behavior, Gunma University Graduate School of Medicine, 3-39-22 Showa-machi, Maebashi, Gunma 371-8511, Japan
[b] Division of Neuropsychiatry, Department of Neuroscience, Yamaguchi University Graduate School of Medicine, 1-1-1 Minamikougushi, Ube, Yamaguchi 755-8505, Japan
[c] Department of Psychiatry and Neuroscience, Gunma University Graduate School of Medicine, 3-39-22 Showa-machi, Maebashi, Gunma 371-8511, Japan

ARTICLE INFO

Article history:
Received 1 May 2014
Received in revised form 13 June 2014
Accepted 14 July 2014
Available online 21 July 2014

Keywords:
Drebrin
Histone acetylation
Histone deacetylase
Dendritic spine
Aβ-derived diffusible ligands
Alzheimer's disease

ABSTRACT

Dendritic spine defects are found in a number of cognitive disorders, including Alzheimer's disease (AD). Amyloid beta (Aβ) toxicity is mediated not only by the fibrillar form of the protein, but also by the soluble oligomers (Aβ-derived diffusible ligands, ADDLs). Drebrin is an actin-binding protein that is located at mature dendritic spines. Because drebrin expression is decreased in AD brains and in cultured neurons exposed to Aβ, it is thought that drebrin is closely associated with cognitive functions. Recent studies show that histone deacetylase (HDAC) activity is elevated in the AD mouse model, and that memory impairments in these animals can be ameliorated by HDAC inhibitors. In addition, spine loss and memory impairment in HDAC2 over-expressing mice are ameliorated by chronic HDAC inhibitor treatment. Therefore, we hypothesized that the regulation of histone acetylation/deacetylation is critical to synaptic functioning. In this study, we examined the relationship between HDAC activity and synaptic defects induced by ADDLs using an HDAC inhibitor, suberoylanilide hydroxamic acid (SAHA). We show that ADDLs reduce the cluster density of drebrin along dendrites without reducing drebrin expression. SAHA markedly increased the acetylation of histone proteins, and it simultaneously attenuated the ADDL-induced decrease in drebrin cluster density. In comparison, SAHA treatment did not affect the density of drebrin clusters or dendritic protrusions in control neurons. Therefore, SAHA likely inhibits ADDL-induced drebrin loss from dendritic spines by stabilizing drebrin in these structures, rather than by increasing drebrin clusters or dendritic protrusions. Taken together, our findings suggest that HDAC is involved in ADDL-induced synaptic defects, and that the regulation of histone acetylation plays an important role in modulating actin cytoskeletal dynamics in dendritic spines under cellular stress conditions, such as ADDL exposure.

1. Introduction

Neuronal activity is known to regulate a complex program of gene expression underlying the structural and functional plasticity of the brain (Flavell and Greenberg, 2008). Chromatin remodeling through histone-tail acetylation is emerging as a fundamental mechanism of gene regulation (Kurdistani and Grunstein, 2003; Goldberg et al., 2007). Histone deacetylases (HDACs) are a class of enzymes that remove acetyl groups from lysine amino acids on a histone, allowing the histones to wrap the DNA more tightly and downregulate gene expression (for review, see Gräff and Tsai, 2013).

Recently, HDAC inhibitors were shown to improve memory and cognitive function in a mouse model of Alzheimer's disease (AD) (Francis et al., 2009; Kilgore et al., 2010). In addition, the reduction in synapse number and the learning impairment in HDAC2 over-expressing mice are ameliorated by chronic treatment with an HDAC inhibitor, suberoylanilide hydroxamic acid (SAHA; vorinostat) (Guan et al., 2009). Furthermore, depression-like behavior induced by chronic mild stress in BALB/c mice is suppressed by chronic administration of SAHA (Uchida et al., 2010).

Various studies indicate that the severity of memory impairment in AD correlates with levels of amyloid beta (Aβ) oligomer, also known as Aβ-derived diffusible ligands (ADDLs) (Lue et al., 1999; Shankar et al., 2007). In addition, it was recently reported that Aβ levels are increased in the brains of patients with

* Corresponding author. Tel.: +81 27 220 8050; fax: +81 27 220 8053.
E-mail address: tshirao@gunma-u.ac.jp (T. Shirao).

http://dx.doi.org/10.1016/j.neuint.2014.07.005
0197-0186/

depression (Kumar et al., 2011). These findings suggest that Aβ is involved in the pathogenesis of neuropsychiatric disorder.

Several studies have shown that expression of drebrin, which stabilizes actin filaments in the dendritic spine (Shirao and González-Billault, 2013), is decreased in AD brains (Harigaya et al., 1996; Counts et al., 2012). Furthermore, it has been reported that a reduction in expression of drebrin A, a neuron-specific isoform, underlies the impairment in activity-dependent glutamate receptor trafficking in an AD animal model (Lee and Aoki, 2012).

Aβ decreases the expression of drebrin both *in vitro* (Zhao et al., 2006; Lacor et al., 2007) and *in vivo* (Harigaya et al., 1996; Counts et al., 2012). Because drebrin is known to be involved in the morphogenesis and maintenance of dendritic spines (Hayashi and Shirao, 1999; Takahashi et al., 2003), the reduction in drebrin expression induced by ADDLs could potentially cause AD pathology, including dendritic spine structural abnormalities and a decrease in spine density (Knafo et al., 2009), resulting in cognitive decline. Histone deacetylation and Aβ-induced drebrin loss may be major factors underlying the pathogenesis of various neuropsychiatric disorders. In this study, we examined whether ADDL-induced changes in drebrin distribution can be attenuated by HDAC inhibition.

2. Materials and methods

2.1. Antibodies

The primary antibodies used in this study include mouse monoclonal antibodies against drebrin (clone M2F6, hybridoma supernatant) (Shirao and Obata, 1985), $A\beta_{1-16}$ (clone 6E10, Covance Inc., Princeton, NJ, USA) and β-actin (clone AC-15; Sigma–Aldrich, St. Louis, MO, USA); rabbit polyclonal antibodies against synapsin I (Merck Millipore, Billerica, MA, USA) and acetyl-histone H3 protein (Lys9/14) (Cell Signaling Technology, Inc., Danvers, MA, USA); and a rabbit monoclonal antibody against histone H3 protein (Cell Signaling Technology, Inc.). The secondary antibodies used for immunocytochemistry were fluorescein-5-isothiocyanate-conjugated goat anti-mouse IgG (MP Biomedicals, LLC-Cappel Products, Santa Ana, CA, USA) and Cy5-conjugated goat anti-rabbit IgG antibodies (Jackson ImmunoResearch, West Grove, PA, USA). The secondary antibodies used for Western blot analysis were horseradish peroxidase (HRP)-conjugated sheep anti-mouse IgG and HRP-conjugated donkey anti-rabbit IgG antibodies (GE Healthcare UK Ltd., Little Chalfont, Buckinghamshire, UK).

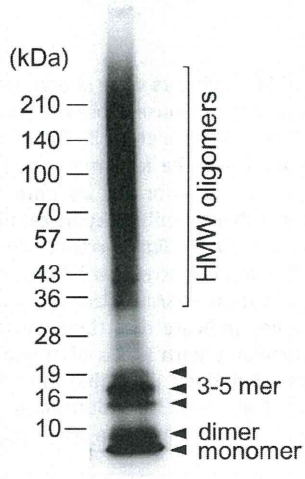

Fig. 1. Western blot analysis of ADDLs. Closed arrowheads show the monomeric to pentameric forms. The broad smear represents high molecular weight (HMW) oligomers (indicated by the bracket).

2.2. Preparation of Aβ-derived diffusible ligands (ADDLs)

$A\beta_{1-42}$ peptide (human sequence) was purchased from Peptide Institute, Inc. (Osaka, Japan). Aβ-derived diffusible ligands (ADDLs) were prepared in accordance with a previously published method, with slight modification (Lambert et al., 2001; Fa et al., 2010). Briefly, $A\beta_{1-42}$ was dissolved in hexafluoro-2-propanol and aliquoted into microcentrifuge tubes. Hexafluoro-2-propanol was completely removed using a SpeedVac centrifuge (Thermo Fisher Scientific Inc., Waltham, MA, USA) at room temperature until a clear peptide film was observed at the bottom of the vials. An aliquot of $A\beta_{1-42}$ was dissolved in anhydrous dimethyl sulfoxide (DMSO) to 5 mM and sonicated in a water bath for 10 min to

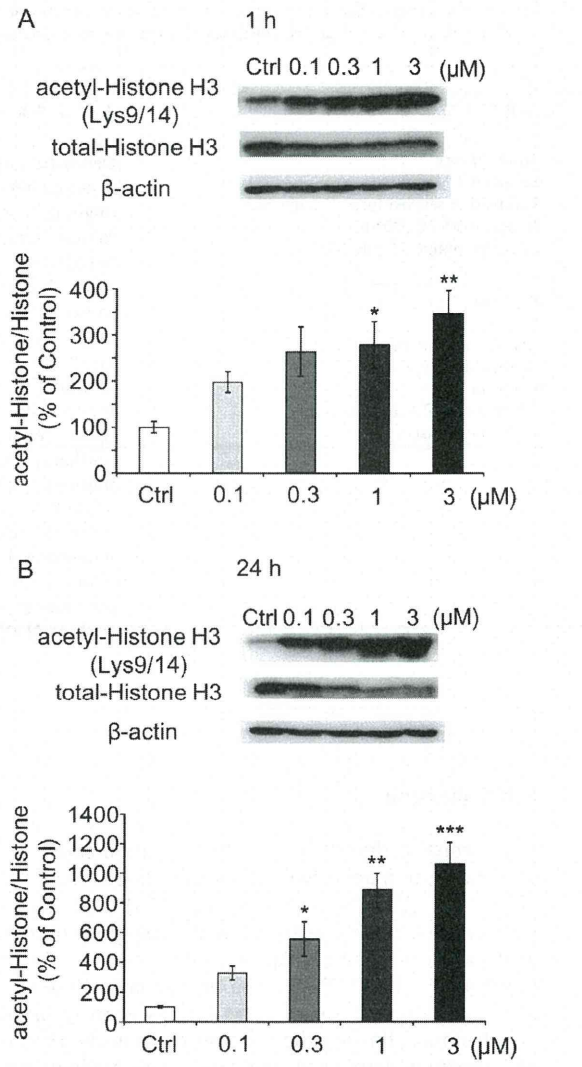

Fig. 2. Effect of SAHA on the acetylation of histone H3 protein assessed with Western blot analysis. Cultured neurons were treated with various dosages of SAHA (0.1, 0.3, 1, 3 μM) for 1 h (A) and 24 h (B). Top panels show typical Western blots of histone H3 protein acetylated at Lys9 and 14. Middle panels show typical Western blots of total histone H3 protein. Bottom panels show β-actin as loading control. Western blots were quantified with NIH ImageJ software after standardizing the ratio of acetyl/total histone H3 protein. Data are presented as means ± SEM, $n = 3$ experiments; $^{*}P < 0.05$ and $^{**}P < 0.01$ vs. control, ANOVA, followed by Dunnett's post hoc test.